Evidence for Isoniazid-Dependent Free Radical Generation Catalyzed by *Mycobacterium tuberculosis* KatG and the Isoniazid-Resistant Mutant KatG(S315T)

Nancy L. Wengenack and Frank Rusnak*

Department of Biochemistry and Molecular Biology and Section of Hematology Research, Mayo Clinic, Rochester, Minnesota 55905

Received November 14, 2000; Revised Manuscript Received April 9, 2001

ABSTRACT: The antitubercular agent isoniazid can be activated by *Mycobacterium tuberculosis* KatG using either a peroxidase compound I/II or a superoxide-dependent oxyferrous pathway. The identity of activated isoniazid is unknown, but it has been suggested that it may be a free radical intermediate. In this work, EPR spin trapping experiments detected isoniazid-derived radicals generated during KatG-mediated oxidation via the peroxidase compound I/II pathway. On the basis of hyperfine splitting patterns and oxygen dependence, these radicals were identified as the acyl, acyl peroxo, and pyridyl radicals of isoniazid. Isoniazid-resistant KatG(S315T) produced the same radicals found with KatG, while the less potent antitubercular agent nicotinic acid hydrazide produced the corresponding nicotinyl radicals. The time course of radical production was similar for KatG and KatG(S315T), while a lower steady-state level of radicals was produced from nicotinic acid hydrazide. These results support an earlier finding that the peroxidase pathway does not correlate with isoniazid resistance conferred by KatG(S315T). Trace amounts of radicals were detected via the superoxide-dependent pathway. The low level of isoniazid-derived radicals found in the superoxide-dependent pathway may be due to scavenging by superoxide.

Tuberculosis (TB) is arguably the greatest scourge to ever afflict mankind, and the destructive path of its causative agent, *Mycobacterium tuberculosis* (*Mtb*), is well-documented throughout history (*1*, *2*). Current reports indicate that this pathogen is responsible for 8 million new infections and 1.5 million deaths annually (*3*). Isoniazid (INH,[1] Figure 1) is a mainstay of tuberculosis chemotherapy, and there is considerable interest in establishing its mechanism of action as a prelude to designing analogues with improved efficacy. The mechanism of INH action involves activation by the *Mtb* enzyme KatG, an iron protoporphyrin IX (heme *b*)-containing enzyme (*4*−*8*) possessing catalase-peroxidase (*5*, *9*−*13*), Mn^{2+}-dependent peroxidase (*14*, *15*), P450-like monooxygenase (*16*), and peroxynitritase (*17*) activities. Previous work demonstrated that INH activation can occur via at least two pathways. The peroxidase compound I/II pathway uses a peroxide (e.g., *t*-BHP) as the oxidant, while a second pathway uses molecular oxygen and produces superoxide that is thought to generate a cytochrome P450-like oxyferrous intermediate at the KatG active site (*12*). Activated INH can subsequently react with other cellular species. Indeed, an isonicotinyl adduct with NAD^+ has been characterized as an inhibitor of the *Mycobacterium smegmatis* InhA protein, an enoyl-acyl carrier protein (ACP) reductase (*18*, *19*). In addition, activated INH forms a covalent but uncharacterized adduct with *Mtb* KasA, a β-ketoacyl ACP synthase (*20*). Both InhA and KasA are involved in fatty acid and mycolic acid biosynthesis. Mycolic acids are unique, vital components of the mycobacterial cell wall.

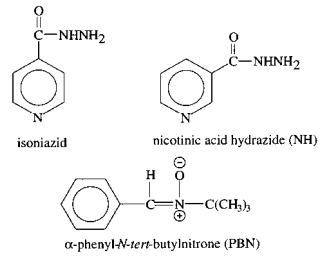

FIGURE 1: (Top) Structures of the antitubercular agent isoniazid and its analogue nicotinic acid hydrazide (NH). (Bottom) Structure of the spin trap α-phenyl-*N*-*tert*-butylnitrone (PBN).

The emergence of isoniazid-resistant strains of *Mtb* highlights the importance of understanding the basis for efficacy in the development of strategies which might circumvent mycobacterial resistance mechanisms. Isoniazid resistance is conferred through mutations in the activating enzyme, KatG, or possibly in the targets of activated isoniazid, InhA and KasA. Most frequent is the KatG(S315T) mutation which is found in 31−92% of isoniazid-resistant clinical isolates of *Mtb* (*21*, *22*), conferring a 10−180-fold increase in the minimal inhibitory concentration (MIC) for isoniazid (*10*, *23*). Isoniazid resistance conferred by *katG(S315T)* is believed to result from a 10-fold (or greater) reduction in the reactivity of the heme with an oxidant (e.g., superoxide) (*12*).

The identity of activated isoniazid has been elusive, but there are several pieces of evidence which indicate that a

* To whom correspondence should be addressed: Section of Hematology Research, Department of Biochemistry and Molecular Biology, Mayo Clinic, 200 First Street, S.W., Rochester, MN 55905. Telephone: (507) 284-4743. Fax: (507) 284-8286. E-mail: rusnak@mayo.edu.

[1] Abbreviations: ACP, acyl carrier protein; DETAPAC, diethyltriaminepentaacetic acid; DPPH, 2,2-diphenyl-1-picrylhydrazyl; EPR, electron paramagnetic resonance; HPLC, high-performance liquid chromatography; HRP, horseradish peroxidase; INH, isoniazid; NH, nicotinic acid hydrazide; MIC, minimal inhibitory concentration; *Mtb*, *Mycobacterium tuberculosis*; NBT, nitro blue tetrazolium; PBN, α-phenyl-*N*-*tert*-butylnitrone; SOD, superoxide dismutase; *t*-BHP, *tert*-butylhydroperoxide.

10.1021/bi002614m CCC: $20.00
Published on Web 06/30/2001

reactive intermediate, formed during KatG-catalyzed oxidation, may be the biocidal form (*9*, *24*−*26*). First, none of the known, stable end products of KatG-mediated isoniazid oxidation (isonicotinic acid, isonicotinamide, pyridine-4-carboxyaldehyde, and 4-pyridylmethanol) have been demonstrated to possess antimycobacterial activity (*27*−*29*). Also, Sinha (*24*) reported that isoniazid-derived free radicals are generated during oxidation by horseradish peroxidase (HRP), while few radicals are found during HRP-mediated oxidation of the less effective antitubercular nicotinic acid hydrazide (NH, Figure 1). Despite structural similarities, NH has a 30-fold higher MIC than isoniazid. EPR spin trapping experiments indicated that several HRP- and isoniazid-dependent free radicals were produced, and these radicals were identified on the basis of EPR spectra as $H^{\bullet}$, $HO^{\bullet}$, $RC(O)^{\bullet}$, and $R^{\bullet}$ (where R represents the pyridine ring of isoniazid). These results suggested that a correlation exists between isoniazid's antimycobacterial activity and its ability to form free radicals. Finally, Shoeb et al. (*25*) found that HRP, isoniazid, and H_2O_2 catalyzed the reduction of nitro blue tetrazolium (NBT), a formazan dye known to react with a variety of reductants, including superoxide and organic radicals.

Thus, the available evidence supports the hypothesis that the active form of isoniazid is a reactive intermediate generated by the enzymatic activity of KatG. In this work, we describe EPR spin trapping experiments conducted to detect for the first time KatG-dependent, isoniazid-derived free radicals. Further, the ability of KatG(S315T) to produce isoniazid-derived radicals was examined to determine if radical production correlates with isoniazid resistance associated with this enzyme.

MATERIALS AND METHODS

Materials. HRP, INH, isonicotinic acid, isonicotinamide, NH, nicotinic acid, nicotinamide, NBT, PBN, SOD, and *t*-BHP were obtained from Sigma Chemical Co. (St. Louis, MO). Diethyltriaminepentaacetic acid (DETAPAC) was obtained from Aldrich Chemical Co. (Milwaukee, WI). The synthesis of [$^{15}N_2$, $^{15}N_3$]-INH has been reported elsewhere (*30*).

Protein Preparation. The expression and purification of recombinant *M. tuberculosis* KatG and KatG(S315T) in *Escherichia coli* has been described previously (*31*). Protein concentrations were determined using Pierce (Rockford, IL) Coomassie plus Protein reagent with bovine serum albumin as the standard (*32*).

Spin Trapping and EPR Detection of Radicals. The structure of the spin trap used in this work, α-phenyl-*N*-*tert*-butylnitrone (PBN), is shown in Figure 1. Solutions containing either 4 mM isoniazid or NH, 10 mM PBN (unless otherwise noted), and 6 μM KatG, KatG(S315T), or HRP were prepared in 50 mM sodium phosphate buffer (pH 7.5). DETAPAC (0.1 mM) was added to chelate adventitious redox active metal ions. Reactions were initiated by addition of 400 μM *t*-BHP, and the solutions were incubated at 37 °C for 30 min unless otherwise noted. After incubation, an aliquot of the reaction was removed and placed in a quartz EPR flat cell (Wilmad Glass, Buena, NJ) for analysis. Anaerobic incubations were carried out under an argon stream, and the flat cell was flushed and filled under argon.

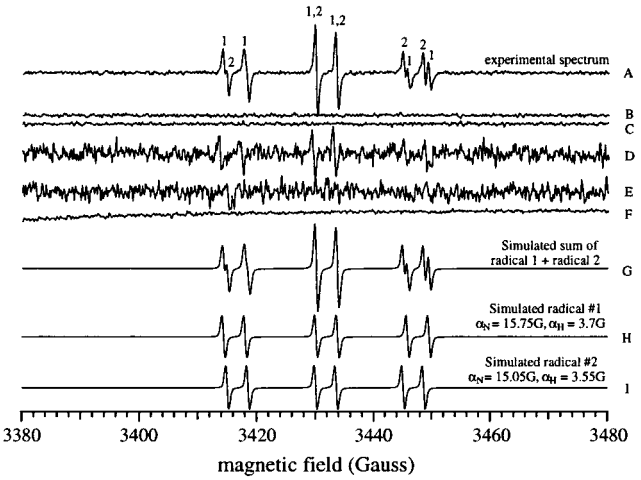

FIGURE 2: EPR spectra of KatG-dependent INH radicals trapped using PBN. Instrument conditions were as follows: microwave frequency, 9.65 GHz; modulation amplitude, 0.33 G; modulation frequency, 100 kHz; power, 20 mW; gain, 2.5×10^5; and temperature, 25 °C. All experimental spectra are the signal-averaged sum of six scans. The intensity scales for all spectra are equivalent. Simulations were done using Bruker Simfonia software (version 1.0) for solution spectra. (A) KatG (6 μM) and INH (4 mM) incubated with 10 mM PBN, 0.1 mM DETAPAC, and 400 μM *t*-BHP in 50 mM sodium phosphate buffer (pH 7.5) for 30 min. (B) Same as for spectrum A except no KatG. (C) Same as for spectrum A except no INH. (D) Same as for spectrum A except no *t*-BHP and the signal intensity was multiplied by 5. (E) Same as for spectrum A except no *t*-BHP, with 0.1 μM SOD, and the signal intensity was multiplied by 5. (F) Same as for spectrum A except no PBN. (G) Spectrum resulting from the addition of a 1:1 ratio of (H) radical adduct 1 and (I) radical adduct 2. (H) Simulation of a carbon- or oxygen-centered radical 1 adducted to PBN using the parameters listed in Table 1. (I) Simulation of a carbon- or oxygen-centered radical 2 adducted to PBN using the parameters listed in Table 1.

EPR spectra were obtained using a Bruker ESP300E spectrometer operating at an X-band frequency at room temperature. Instrument conditions for all analyses were as follows: microwave frequency, 9.65 GHz; modulation amplitude, 0.33 G; modulation frequency, 100 kHz; power, 20 mW; gain, 2.5×10^5; and temperature, 25 °C. All spectra are the signal-averaged sum of six scans unless otherwise noted. All reactions were carried out in triplicate.

Reported *g* values were determined relative to the standard DPPH ($g = 2.0037 \pm 0.0002$) using the equation

$$g_x - g_{\mathrm{Std}} = -\frac{B_x - B_{\mathrm{Std}}}{B_{\mathrm{Std}}} g_{\mathrm{Std}}$$

where g_x is the *g* value of the unknown, g_{Std} is the *g* value of DPPH, B_x is the center field position of the unknown, and B_{Std} is the center field position of the DPPH EPR spectrum (*33*).

RESULTS

Spin Trapping of KatG-Dependent, Isoniazid-Derived Radicals. Figure 2 shows EPR spectra of KatG-dependent, isoniazid-derived radicals that were trapped by PBN. Control reactions lacking KatG (Figure 2B) or isoniazid (Figure 2C) did not generate radical adducts, demonstrating a requirement for both in radical generation. Reactions which lacked *t*-BHP (Figure 2D) produced radical adducts with significantly

diminished intensity relative to that depicted in Figure 2A. This indicates that (1) *t*-BHP-dependent catalysis, likely via the peroxidase compound I/II pathway, is responsible for the majority of radical adduct formation represented by Figure 2A and (2) some non-peroxide-dependent radical adduct formation occurs as evidenced by the small signal seen in the absence of *t*-BHP (Figure 2D). The addition of SOD to the reaction mixture described in the legend of Figure 2A had no effect on the adduct producing Figure 2A (data not shown), further implicating a peroxide-dependent, and not superoxide-dependent, pathway for the large adduct signal seen in Figure 2A. The non-*t*-BHP-dependent radical adducts represented in Figure 2D are likely formed via a superoxide-dependent pathway since addition of SOD to the reaction mixture in the absence of *t*-BHP (Figure 2E) eliminated the small signal seen in Figure 2D. This also eliminates the possibility that some contaminating H_2O_2 is responsible for the small radical adduct signal seen in Figure 2D. Spectra of reactions lacking PBN were devoid of radical adduct spectra (Figure 2F).

The spectrum in Figure 2A consists of three sets of doublets with an approximate intensity ratio of 1:2:1. Adduct formation between PBN and a single radical (lacking $I \neq 0$ nuclei) would be expected to produce a six-line spectrum consisting of both nitrogen and hydrogen hyperfine splitting with a 1:1:1 intensity ratio of doublets. To account for the features in Figure 2A, we hypothesize that it consists of two PBN radical adducts with similar, but not identical, hyperfine splitting constants. Computer simulations (Figure 2H,I) and addition of equal quantities of the two proposed radical adducts produce a composite spectrum (Figure 2G) that adequately reproduces the experimental spectrum (Figure 2A). The individual radical adducts are designated as radical adduct 1 or radical adduct 2 with their contributions noted above the spectrum in Figure 2A. Although additional assignments for the identity of the species which contribute to the composite spectrum are possible, we hypothesize that two stable PBN−radical adducts, whose hyperfine parameters are listed in Table 1, generate these spectra. Additional evidence presented below is consistent with this assignment.

The six-line spectrum of Figure 2A suggests that the isoniazid radicals formed are either carbon- or oxygen-centered, but not nitrogen-centered, since additional splitting would be expected between the unpaired electron and the N atom derived from either of the hydrazine nitrogens of isoniazid. The small splitting seen in the high-field doublets of Figure 2A is not likely to result from a nitrogen-centered radical since the middle set of doublets does not show the same splitting and only two distinct lines are observed. Further support for the idea of carbon- or oxygen-centered radicals was obtained using an isotopically labeled substrate (Figure 3). The use of [$^{15}N_2$,$^{15}N_3$]isoniazid in the trapping reaction confirmed that the adducts do not result from a nitrogen-centered radical derived from isoniazid. ^{15}N has a nuclear spin I of $^1/_2$ in contrast to ^{14}N which has an I of 1 . Therefore, a decrease in the number of hyperfine lines would be predicted in the presence of ^{15}N-labeled isoniazid if a nitrogen-centered radical were trapped by PBN. Figure 3 indicates that trapping experiments conducted using ^{15}N-labeled isoniazid (A) gave a spectrum identical to that of ^{14}N-labeled isoniazid (B).

Table 1: Hyperfine Splitting Constants for INH and NH Radical Adducts

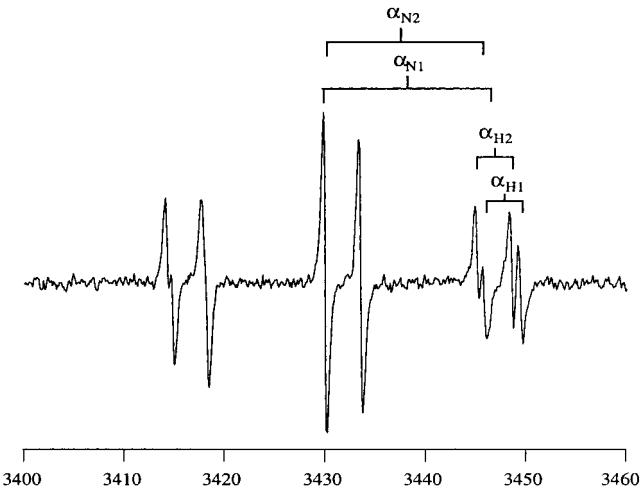

		hyperfine splitting constant[a] (G)			
		radical 1		radical 2	
enzyme	g value[b]	α_{N1}	α_{H1}	α_{N2}	α_{H2}
Isonicotinic Acid Hydrazide					
wild-type KatG	1.9996	15.8 ± 0.1	3.7 ± 0.1	15.1 ± 0.1	3.6 ± 0.1
KatG(S315T)	1.9996	15.9 ± 0.1	3.8 ± 0.1	15.0 ± 0.1	3.5 ± 0.1
HRP	1.9996	15.7 ± 0.1	3.8 ± 0.0	ND[c]	ND[c]
Nicotinic Acid Hydrazide					
wild-type KatG	1.9997	15.9 ± 0.0	3.8 ± 0.1	15.1 ± 0.0	3.4 ± 0.0
KatG(S315T)	1.9997	15.9 ± 0.0	3.8 ± 0.0	15.1 ± 0.0	3.4 ± 0.1
HRP	1.9997	15.9 ± 0.1	3.8 ± 0.1	15.0 ± 0.1	3.3 ± 0.2

[a] Mean ± standard deviation of three trials; hyperfine constants were determined from the experimental spectra using the pattern shown in the above figure. [b] Determined relative to the standard DPPH (g = 2.0037 ± 0.0002). [c] Not detected.

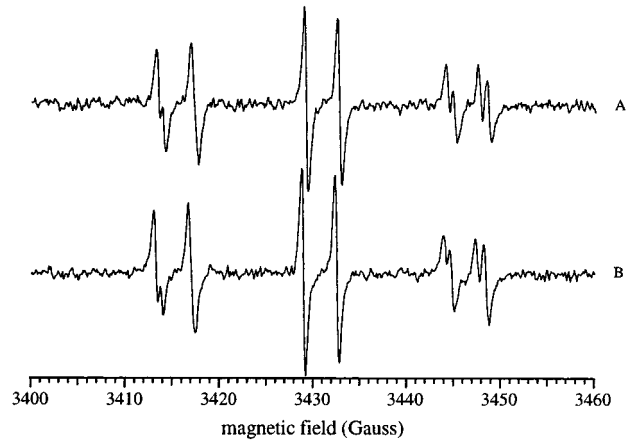

FIGURE 3: EPR spectra of [$^{14}N_2$,$^{14}N_3$]-INH− vs those of [$^{15}N_2$,$^{15}N_3$]-INH−PBN adducts. Instrument conditions were the same as described in the legend of Figure 2. Solutions contained 6 μM KatG, 4 mM INH, 10 mM PBN, 0.1 mM DETAPAC, and 400 μM *t*-BHP in 50 mM sodium phosphate buffer (pH 7.5). Solutions were incubated at 37 °C for 30 min. Spectra are the signal-averaged sum of six scans: (A) [$^{14}N_2$,$^{14}N_3$]-INH and (B) [$^{15}N_2$,$^{15}N_3$]-INH.

Anaerobic versus Aerobic Radical Adduct Production. Spin trapping with PBN under anaerobic conditions (Figure 4A) generated a six-line spectrum consisting of a triplet of doublets with a 1:1:1 intensity and no additional splitting of the outer doublets. This adduct has a g value (2.0002) and

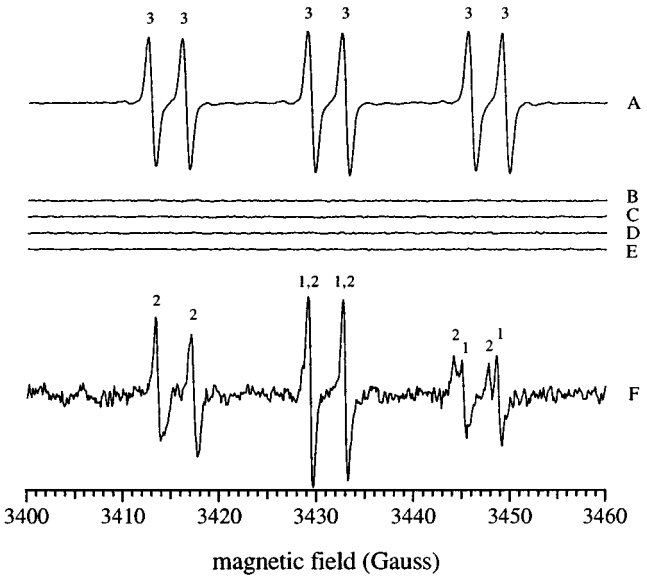

FIGURE 4: EPR spectra of INH−PBN adducts under anaerobic and aerobic conditions. Instrument conditions were the same as those described in the legend of Figure 2 except the intensity is 48 times larger than that of Figure 2. (A) The solution contained 6 μM KatG along with 4 mM INH, 10 mM PBN, 0.1 mM DETAPAC, and 400 μM *t*-BHP in 50 mM sodium phosphate buffer (pH 7.5) and was incubated at 37 °C for 30 min under anaerobic conditions. (B) Same as for spectrum A except no KatG. (C) Same as for spectrum A except no isoniazid. (D) Same as for spectrum A except no PBN. (E) Same as for spectrum A except no *t*-BHP. (F) Sample used for spectrum A after exposure to O_2 for 30 min. The spectrum is the signal-averaged sum of six scans, and the intensity was multiplied by 8 for comparison with spectrum A.

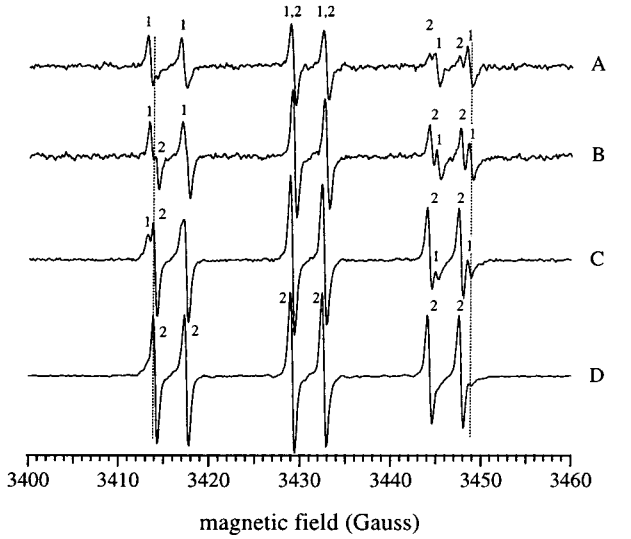

FIGURE 5: EPR spectra of KatG-dependent INH−PBN adducts in the presence of varying amounts of PBN. The solutions contained 6 μM KatG along with 4 mM INH, 0.1 mM DETAPAC, 400 μM *t*-BHP, and PBN at the indicated concentrations in 50 mM sodium phosphate buffer (pH 7.5). All solutions were incubated at 37 °C for 30 min. The spectra are the signal-averaged sum of six scans. Instrument conditions were the same as those described in the legend of Figure 2. (A) With 5 mM PBN; the signal intensity is multiplied by 4 for comparison with spectrum D. (B) With 10 mM PBN; the signal intensity is multiplied by 4 for comparison with spectrum D. (C) With 20 mM PBN; the signal intensity is multiplied by 2 for comparison with spectrum D. (D) With 40 mM PBN.

hyperfine splitting constants (α_N = 16.5 G, α_H = 3.6 G) which differ from those of both radical adduct 1 and radical adduct 2 (Table 1). This suggests a third species can be

Scheme 1

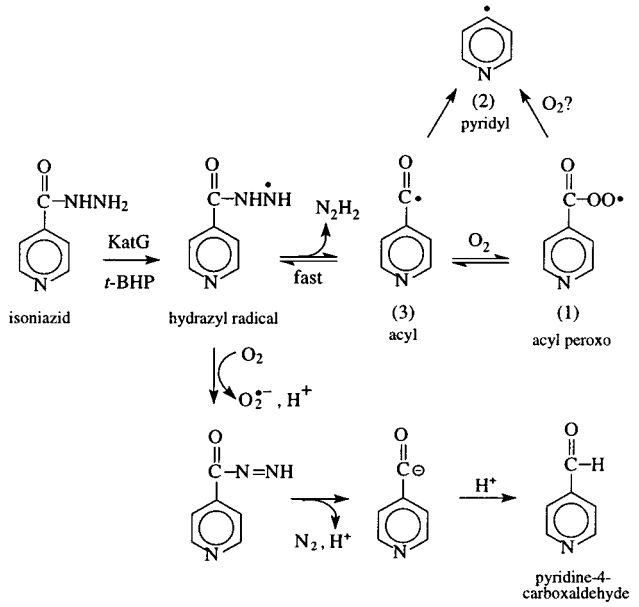

trapped under anaerobic conditions (radical adduct 3) and that formation of radical adducts 1 and 2 may be oxygen-dependent. Control reactions lacking KatG (Figure 4B), isoniazid (Figure 4C), PBN (Figure 4D), and *t*-BHP (Figure 4E) demonstrated the dependence of radical formation on each of these components. The spectrum of radical adduct 3 disappeared upon exposure of the reaction mixture to oxygen and was replaced with the spectrum representing radical adducts 1 and 2 (Figure 4F). The magnitude of the signal seen under anaerobic conditions was much larger than that under aerobic conditions, suggesting that oxygen readily promotes destruction of radical adduct 3 and production of radical adducts 1 and 2. An alternative explanation may be that the spectra of radical adducts 1 and 2 are hidden under the more intense spectrum of radical adduct 3 and become visible only after the O_2-dependent destruction of radical adduct 3.

From these and subsequent data, we hypothesize that radical adducts 1−3 are derived from the radicals shown in Scheme 1. Although definitive proof of these species is tenuous, these and other data presented herein, as well as other published work (*9*), are consistent with this assignment. It is possible that the radicals formed are nitrogen-centered, but the N_β hyperfine coupling constant is very small. This is not likely since PBN−nitrogen-centered radical adducts typically have N_β hyperfine constants of >0.88 G, with most having N_β hyperfine constants in the range of 1.5−3 G (*34*).

Effect of Varying the Spin Trap Concentration on Trapped Radical Adducts. The EPR spectra shown in Figure 5 demonstrate the effect of varying the spin trap concentration on the pattern of trapped radical adducts. In the presence of 5 mM PBN (Figure 5A), a mixture of radical adducts 1 and 2 is seen. As the concentration of PBN is increased to 10 (B), 20 (C), and 40 mM (D), the ratio of the two trapped radical adducts changes as evidenced by the increased intensity of the inner pair of hyperfine lines in each spectrum. At the highest concentration of PBN, the signal exhibits a 1:1:1 hyperfine pattern reflecting the presence of primarily radical adduct 2. Increasing the spin trap concentration increases the probability that radical 2 will encounter the

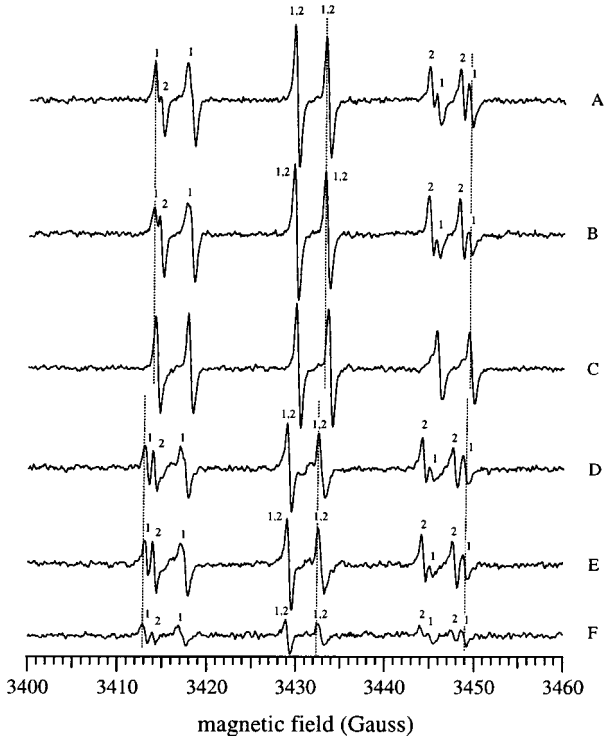

FIGURE 6: EPR spectra of INH− and NH-derived radical−PBN adducts generated by KatG, KatG(S315T), and HRP. Instrument conditions were the same as those described in the legend of Figure 2. All solutions contained 10 mM PBN, 0.1 mM DETAPAC, and 400 μM *t*-BHP in 50 mM sodium phosphate buffer (pH 7.5) and were incubated at 37 °C for 30 min prior to analysis. All spectra are the signal-averaged sum of six scans, and the intensity scales are equivalent: (A) 6 μM KatG and 4 mM INH, (B) 6 μM KatG-(S315T) and 4 mM INH, (C) 6 μM HRP and 4 mM INH, (D) 6 μM KatG and 4 mM NH, (E) 6 μM KatG(S315T) and 4 mM NH, and (F) 6 μM HRP and 4 mM NH.

spin trap and form a stable adduct before it can undergo solution-mediated decay.

Isoniazid- and NH-Dependent Radical Adducts Produced by KatG(S315T) and HRP. EPR spectra of isoniazid- and nicotinic acid hydrazide-dependent PBN adducts generated by KatG, KatG(S315T), and HRP under aerobic conditions are shown in Figure 6, with the hyperfine splitting constants given in Table 1. KatG(S315T) produces isoniazid-derived radical adducts which are nearly identical to those produced by KatG (compare spectra A and B of Figure 6). The splitting pattern and intensity ratio suggest the presence of two radical adducts with hyperfine constants similar to those found for the KatG-dependent, isoniazid-derived radical adducts. The only discernible difference is that KatG(S315T) produces a radical 2:radical 1 adduct ratio slightly different from that of KatG. Isoniazid-derived radical adducts generated by HRP are shown in Figure 6C. The HRP-generated spectrum indicates formation of primarily a single radical adduct that has hyperfine constants identical to those of radical adduct 1.

PBN−radical adducts derived from the less potent antitubercular agent nicotinic acid hydrazide (NH) were also detected by EPR and can be seen in Figure 6D−F. KatG produced a NH−PBN adduct spectrum which was very much like that derived from isoniazid except for a slight shift in the *g* value (compare panels D and A of Figure 6). The hyperfine patterns and splitting constants (Table 1) were

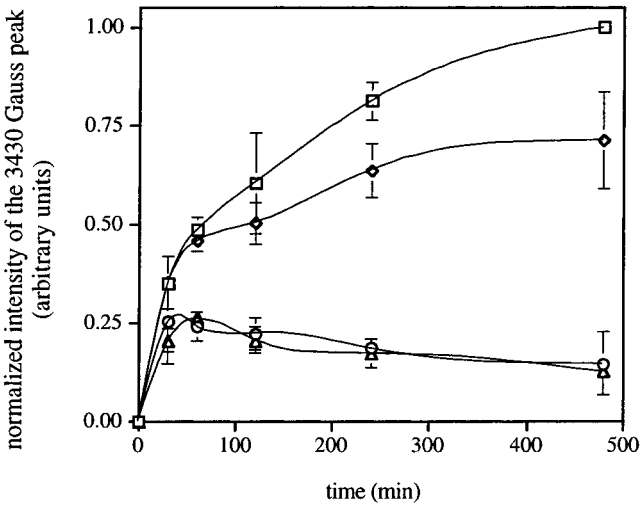

FIGURE 7: Time course of INH− and NH radical−PBN adduct production. The solutions contained 6 μM KatG or KatG(S315T), 4 mM INH or NH, 10 mM PBN, 0.1 mM DETAPAC, and 400 μM *t*-BHP in 50 mM sodium phosphate buffer (pH 7.5). All solutions were incubated at 37 °C for 30 min, and samples were removed at various time points for EPR analysis. Instrument conditions were the same as those described in the legend of Figure 2. Error bars represent the standard deviation of triplicate experiments. Normalized intensity is the intensity of the 3430 G peak at time *t* divided by the intensity at 8 h for the sample of KatG and isoniazid. Lines represent interpolation of the data points: (□) KatG and INH, (◇) KatG(S315T) and INH, (○) KatG and NH, and (△) KatG(S315T) and NH.

nearly identical, suggesting that radical adduct 1 and radical adduct 2 of NH were formed. The other notable difference was a decrease in the intensity of the NH-derived radical spectra relative to the intensity of the isoniazid-derived radical spectra. KatG(S315T) also produced NH-derived adduct spectra with a hyperfine pattern and splitting constants identical to those derived from INH (compare panels E and B of Figure 6). HRP produced similar NH-derived radical adduct spectra, although the signal intensity, and therefore the steady-state level, of the generated radical adduct was low (Figure 6F). Together, the results suggest that KatG and KatG(S315T) can produce radical adduct 1 and radical adduct 2 from both isoniazid and NH.

Time Course and Stability of Radical Adduct Production. The differing intensities of radical adduct spectra seen in Figure 6 suggested that there may be differences in either the amount or the rate of isoniazid and NH radical formation and/or decomposition. Therefore, an examination of the time course and total amount of isoniazid and NH-derived adducts produced by KatG and KatG(S315T) was undertaken. Figure 7 indicates that the amount of isoniazid-derived radical adduct produced by KatG increases continually throughout the 8 h study period. For the first hour, the amount of isoniazid-derived radical adduct produced by KatG(S315T) is equivalent to that generated by KatG. After 1 h, the adducts generated by KatG(S315T) reach a steady state which is roughly 25% lower than that of KatG over the remaining 7 h. In contrast, NH-derived adducts produced by KatG and KatG(S315T) reach a peak intensity after 30 min which is diminished relative to the amount of isoniazid-derived radicals produced and slowly declines over time. After 60 min, the absolute levels of NH-derived adducts are 2−4-fold lower than the isoniazid-derived adduct levels. The 8 h time course indicates a relatively slow reaction. Previous

work has demonstrated that isoniazid oxidation by KatG is a slow process ($k_{cat} = 0.0022\ s^{-1}$) relative to the catalase ($k_{cat} = 5800\ s^{-1}$) and peroxidase ($k_{cat} = 2\ s^{-1}$) activities of KatG (*12*, *31*). Therefore, given the concentrations of the reactants that were used, neither INH nor *t*-BHP was limiting during the 8 h study. It should be noted that the decay rate, and therefore the stability, of the radical adducts is not well understood.

DISCUSSION

The prevailing hypothesis regarding isoniazid's mechanism of action proposes that isoniazid-derived free radicals generated by KatG are responsible for the inactivation of cellular targets such as InhA and KasA (*9*, *20*, *35*). Sinha (*24*, *36*) has reported detection of carbon-centered, isoniazid-derived radicals generated by HRP and assigned one of these radicals as the acyl radical of isoniazid on the basis of its hyperfine patterns. This paper reports for the first time detection of isoniazid-derived acyl radical adduct 3, acyl peroxo radical adduct 1, and pyridyl radical adduct 2 generated by *Mtb* KatG. EPR radical adduct spectra generated in the presence of PBN indicate that two carbon- or oxygen-centered radicals which lack attached hydrogens are formed during KatG-mediated isoniazid oxidation, based on the hyperfine patterns and intensities. The use of [^{15}N]INH had no effect on the hyperfine splitting, supporting the assignment of carbon- or oxygen-centered radicals. Further, anaerobic conditions led to generation of only a single radical adduct which was assigned as deriving from the acyl radical. Exposure to oxygen then led to formation of the two additional radical adducts. Increasing the concentration of the spin trap led to a better trapping efficiency for the pyridyl radical which otherwise appears to decay rapidly in solution. Formation of radical adducts 1−3 was dependent upon the presence of *t*-BHP in the reaction mixture, suggesting that the radicals were formed via the peroxidase compound I/II pathway. In addition, weak radical adduct signals were observed in the absence of *t*-BHP and are purported to arise via the superoxide-dependent pathway.

Interestingly, KatG(S315T) also produced radical adducts 1 and 2 from isoniazid. The hyperfine splitting constants and parameters were identical to those found for KatG-derived radical adducts, and as for KatG, formation of these radical adducts by KatG(S315T) required *t*-BHP, indicating they were formed via the peroxidase compound I/II pathway. In addition, both KatG and KatG(S315T) produced analogous radical adducts from the less effective antitubercular nicotinic acid hydrazide via the peroxidase compound I/II pathway. The finding that the resistant enzyme KatG(S315T) and the ineffective antitubercular NH produce radical adducts comparable to those produced by KatG and isoniazid suggests that the radical adducts generated from the KatG- and peroxide-dependent oxidation of isoniazid do not correlate with in vivo susceptibility to the drug. This result is consistent with our previous report that isoniazid oxidation via the KatG peroxidase pathway does not correlate with isoniazid susceptibility (*12*).

The time course of radical adduct production by KatG and KatG(S315T) shows some intriguing differences. KatG(S315T) is slightly less adept at generating the isoniazid-derived free radicals than KatG; however, the difference is less than 2-fold. This correlates nicely with the kinetic parameters for both enzymes reported previously which indicated that KatG(S315T) is a competent catalase-peroxidase with a catalytic efficiency near that of KatG (*12*). Therefore, one would predict that KatG(S315T) should produce nearly the same amount of radicals as KatG via the peroxidative pathway using a peroxide (e.g., *t*-BHP) as the oxidant. The amount of radical adduct species produced from NH by both KatG and KatG(S315T) is 2−4-fold lower over extended periods of time than from isoniazid. This is not the result of a reduced initial rate of oxidation since a previous report indicated that NH is oxidized as rapidly as isoniazid via the peroxidative pathways of KatG and KatG(S315T) (*12*). Therefore, these results may be consistent with a gradual inhibition of KatG by NH or some metabolite of NH. Mechanism-based inhibition of heme proteins by hydrazines has been demonstrated previously by Ator and co-workers (*37*), who found meso-alkylated heme following the inactivation of HRP with alkylhydrazines. Further, Johnsson and Schultz (*9*) suggested that both isoniazid and NH acted as an inhibitor of KatG catalase activity but that NH was a more effective inhibitor than isoniazid. The time course results are consistent with this interpretation. Therefore, it is possible that isoniazid is a more potent antitubercular than NH because it is a less potent inhibitor of KatG, thereby allowing KatG to activate isoniazid for longer periods than NH.

Although free radicals generated via the peroxidase pathway do not correlate with isoniazid susceptibility, it is possible that free radicals generated via the KatG superoxide-dependent pathway are responsible for the activity of isoniazid. In this work, significant amounts of radical adducts were detected only when the peroxidase substrate *t*-BHP was used. Further, the presence of superoxide dismutase had no effect on the reaction mixture used to generate Figure 2A, confirming that *t*-BHP, and not superoxide, was required for the majority of the radical adduct spectrum seen in Figure 2A. Substitution of the superoxide-generating system (xanthine with xanthine oxidase) for *t*-BHP in the Figure 2A mixture produced trace amounts of radicals (data not shown). Also, addition of SOD to reaction mixtures lacking *t*-BHP (Figure 2E) eliminated the small non-peroxide-dependent radical adduct signal seen in Figure 2D, suggesting that some superoxide-mediated radical production occurs. Additionally, the same stable end products of KatG-mediated, isoniazid oxidation are generated by both the peroxide- and superoxide-dependent pathways (*12*). This suggests that a common reaction mechanism is utilized, and therefore, similar radical intermediates should be formed via these pathways. The lack of significant radical−PBN adduct spectra in the absence of peroxide may therefore be due to competing destruction of the INH radical by superoxide. Since the rate of isoniazid oxidation by KatG via the superoxide pathway is at least 10-fold higher than that of KatG(S315T) (*12*), it would follow that at least 10-fold more radicals should be produced via this pathway by KatG than by KatG(S315T). Therefore, the increased rate of isoniazid oxidation via the superoxide pathway is likely to be crucial for formation of large amounts of activated isoniazid relative to that produced by the peroxidase pathway. Cellular targets such as InhA and KasA may effectively compete with superoxide for reaction with activated INH. Alternatively, the superoxide pathway may

generate nonradical intermediates (e.g., an acyl anion or acylium ion).

It is tempting to speculate that diverting isoniazid oxidation through the peroxidase, rather than the superoxide-dependent, pathway may be a way of overcoming isoniazid resistance in strains of *Mtb* possessing KatG(S315T). Utilizing the peroxidase pathway, the two enzymes generate the same intermediates (from this work) in similar quantities at similar rates (*12*). Enhancement of the peroxidase pathway by synergistic treatment with isoniazid with a second compound which stimulates intracellular H_2O_2 production may be able to alleviate isoniazid resistance in *Mtb* harboring KatG(S315T).

ACKNOWLEDGMENT

We thank Smilja Todorovic for providing [^{15}N]INH.

REFERENCES

1. Ryan, F. (1993) in *The Forgotten Plague. How the Battle Against Tuberculosis Was Won-and Lost*, Little, Brown & Company, Boston.
2. Daniel, T. M., Bates, J. H., and Downes, K. A. (1994) in *Tuberculosis. Pathogenesis, Protection, and Control* (Bloom, B. R., Ed.) pp 13−24, American Society for Microbiology Press, Washington, DC.
3. World Health Organization (1999) in *World Health Report*, Geneva.
4. Middlebrook, G. (1954) *Am. Rev. Tuberc. 69*, 471−472.
5. Gayathri Devi, B., Shaila, M. S., Ramakrishnan, T., and Gopinathan, K. P. (1975) *Biochem. J. 149*, 187−197.
6. Zhang, Y., Heym, B., Allen, B., Young, D., and Cole, S. (1992) *Nature 358*, 591−593.
7. Zhang, Y., Garbe, T., and Young, D. (1993) *Mol. Microbiol. 8*, 521−524.
8. Johnsson, K., Froland, W. A., and Schultz, P. G. (1997) *J. Biol. Chem. 272*, 2834−2840.
9. Johnsson, K., and Schultz, P. G. (1994) *J. Am. Chem. Soc. 116*, 7425−7426.
10. Heym, B., Alzari, P. M., Honoré, N., and Cole, S. T. (1995) *Mol. Microbiol. 15*, 235−245.
11. Marcinkeviciene, J. A., Magliozzo, R. S., and Blanchard, J. S. (1995) *J. Biol. Chem. 270*, 22290−22295.
12. Wengenack, N. L., Hoard, H. M., and Rusnak, F. (1999) *J. Am. Chem. Soc. 121*, 9748−9749.
13. Saint-Joanis, B., Souchon, H., Wilming, M., Johnsson, K., Alzari, P. M., and Cole, S. T. (1999) *Biochem. J. 338*, 753−760.
14. Magliozzo, R. S., and Marcinkeviciene, J. A. (1997) *J. Biol. Chem. 272*, 8867−8870.
15. Zabinski, R. F., and Blanchard, J. S. (1997) *J. Am. Chem. Soc. 119*, 2331−2332.
16. Magliozzo, R. S., and Marcinkeviciene, J. A. (1996) *J. Am. Chem. Soc. 118*, 11303−11304.
17. Wengenack, N. L., Jensen, M. P., Rusnak, F., and Stern, M. K. (1999) *Biochem. Biophys. Res. Commun. 256*, 485−487.
18. Banerjee, A., Dubnau, E., Quemard, A., Balasubramanian, V., Um, K. S., Wilson, T., Collins, D., de Lisle, G., and Jacobs, W. R., Jr. (1994) *Science 263*, 227−230.
19. Vilcheze, C., Morbidoni, H. R., Weisbrod, T. R., Iwamoto, H., Kuo, M., Sacchettini, J. C., and Jacobs, W. R., Jr. (2000) *J. Bacteriol. 182*, 4059−4067.
20. Mdluli, K., Slayden, R. A., Zhu, Y., Ramaswamy, S., Pan, X., Mead, D., Crane, D. D., Musser, J. M., and Barry, C. E., III (1998) *Science 280*, 1607−1610.
21. Musser, J. M., Kapur, V., Williams, D. L., Kreiswirth, B. N., van Soolingen, D., and van Embden, J. D. A. (1996) *J. Infect. Dis. 173*, 196−202.
22. Ramaswamy, S., and Musser, J. M. (1998) *Tuberc. Lung Dis. 79*, 3−29.
23. Rouse, D. A., DeVito, J. A., Li, Z., Byer, H., and Morris, S. L. (1996) *Mol. Microbiol. 22*, 583−592.
24. Sinha, B. K. (1983) *J. Biol. Chem. 258*, 796−801.
25. Shoeb, H. A., Bowman, B. U., Jr, Ottolenghi, A. C., and Merola, A. J. (1985) *Antimicrob. Agents Chemother. 27*, 408−412.
26. Shoeb, H. A., Bowman, B. U., Jr, Ottolenghi, A. C., and Merola, A. J. (1985) *Antimicrob. Agents Chemother. 27*, 404−407.
27. Quemard, A., Lacave, C., and Laneelle, G. (1991) *Antimicrob. Agents Chemother. 35*, 1035−1039.
28. Seydel, V. J. K., Wempe, E., and Nestler, H. J. (1968) *Arzneim.-Forsch. 18*, 362−367.
29. Seydel, J. K., Schaper, K.-J., Wempe, E., and Cordes, H. P. (1976) *J. Med. Chem. 19*, 483−492.
30. Todorović, S., Juranić, N., Macura, S., and Rusnak, F. (1999) *J. Am. Chem. Soc. 121*, 10962−10966.
31. Wengenack, N. L., Uhl, J. R., St. Amand, A. L., Tomlinson, A. J., Benson, L. M., Naylor, S., Kline, B. C., Cockerill, F. R., III, and Rusnak, F. (1997) *J. Infect. Dis. 176*, 722−727.
32. Bradford, M. M. (1976) *Anal. Biochem. 72*, 248−254.
33. Weil, J. A., Bolton, J. R., and Wertz, J. E. (1994) in *Electron Paramagnetic Resonance: Elementary Theory and Practical Applications*, Wiley, New York.
34. Li, A. S. W., Cummings, K. B., Roethling, H. P., and Buettner, G. R. (1988) *J. Magn. Reson. 39*, 140−142.
35. Shoeb, H. A., Bowman, B. U., Jr, Ottolenghi, A. C., and Merola, A. J. (1985) *Antimicrob. Agents Chemother. 27*, 399−403.
36. Kalyanaraman, B., and Sinha, B. K. (1985) *Environ. Health Perspect. 64*, 179−184.
37. Ator, M. A., David, S. K., and Ortiz de Montellano, P. R. (1989) *J. Biol. Chem. 264*, 9250−9257.

BI002614M